Reactive and Functional Polymers 97 (2015) 77–85

Contents lists available at ScienceDirect

Reactive and Functional Polymers

journal homepage: www.elsevier.com/locate/react

Effect of functional groups on physicochemical and mechanical behavior of biocompatible macroporous hydrogels

Rebeca E. Rivero [a], Fabrisio Alustiza [a,b], Nancy Rodríguez [b], Pablo Bosch [b], María C. Miras [a], Claudia R. Rivarola [a], Cesar A. Barbero [a,*]

[a] Chemistry Department, Faculty of Exact, Physical-Chemical and Natural Sciences, National University of Río Cuarto, National Route 36 KM 601, X5804ZAB Rio Cuarto, Cordoba, Argentina
[b] Molecular Biology Department, Faculty of Exact, Physical-chemical and Natural Sciences, National University of Río Cuarto, National Route 36 Km 601, X5804ZAB Rio Cuarto, Cordoba, Argentina

ARTICLE INFO

Article history:
Received 31 July 2015
Received in revised form 15 October 2015
Accepted 17 October 2015
Available online 19 October 2015

Keywords:
Macroporous hydrogel
Mechanical anisotropy
Cryogelation
Water states
Fibroblasts

ABSTRACT

The increasing interest in studying the properties of biocompatible hydrogels is due to their possible applications in bioengineering. Properties of hydrogels based on N-isopropylacrylamide (NIPAM) and the effect caused by copolymerization with 2-acrylamido-2-methylpropanesulfonic acid (AMPS) or N-acryloyl-tris-(hydroxymethyl)aminomethane (HMA) were investigated. Hydrogels were synthesized by free radical polymerization at room temperature or by cryogelation at −18 °C. The presence of different functional groups (isopropyl, $-SO_3^-$, and –OH) and thermal conditions of polymerization affected the morphology and physicochemical and mechanical properties of hydrogels. Scanning electron microscopy (SEM) revealed the presence of macropores created by cryogelation with the morphology of the pores dependent on chemical composition of the copolymer. Poly(NIPAM-co-HMA) has spherical and isolated pores, whereas PNIPAM and Poly(NIPAM-co-AMPS) showed ellipsoidal interconnected pores. Three different water states were detected by differential scanning calorimetry (DSC), indicating the presence of nano- and macropores. Elastic modulus (E) was measured to be around 3–6.5 kPa by uniaxial compression. However, higher E values (20–30 kPa) and an anisotropic mechanical response were observed for PNIPAM and PNIPAM-co-AMPS hydrogels with ellipsoidal pores, a behavior that is almost similar to that of cartilage and bone tissues. Cytocompatibility studies using bovine fibroblasts (BFs) indicated good cell attachment and proliferation on PNIPAM-based hydrogel surfaces, although initially the cell adhesion varied depending on the composition of the surface. These hydrogels could be an interesting choice for the development of scaffolds in tissue engineering.

1. Introduction

Hydrogels are cross-linked macromolecules with high capacity to absorb aqueous solutions because of the hydrophilic characters of their functional groups. Cross-linked polymers usually contain nanoscale pores [1] in swollen state, whereas the macroporous hydrogel counterparts are characterized by their microscale pores that remain unchanged in both swollen and dried states. One of the disadvantages of porous hydrogels is their poor mechanical performance in swollen state, which restricts their potential applications. Many methods for building materials with enhanced mechanical properties have been proposed [2–4], for example, interpenetrating or nanocomposite systems based on matrix hydrogels [5–7] as well as macroporous hydrogels prepared by different methods, including cryogelation [8–10].

Porous materials, particularly hydrogels, are important engineered tissue scaffolds, because their structure allows cellular migration and proliferation [11–14]. These cell-populated scaffolds could be subsequently used to graft or replace soft or hard tissues such as cartilage or bone. For that purpose, a particular porous hydrogel should have the following basic structural characteristics: (i) sufficient mechanical strength to resist pressure after grafting, (ii) high porosity with suitable pore size and highly interconnected pore structure to allow cellular colonization and biologic fluid movement, and (iii) a large surface area that favors cell adhesion and propagation.

In addition, hydrogels that are sensitive to external parameters such as pH, temperature, ionic force, and electric field have been reported [15,16]. These materials, known as “smart hydrogels” respond to specific micro environmental changes by a reversible phase transition, from swollen to collapsed state. It has been demonstrated that during the collapse, the hydrogel expels the solution trapped inside, a property that is proved to be useful for many biomedical applications, such as drug release system [17], contact lenses [18], corneal implants [19], artificial menisci [20], and others [21-27].

* Corresponding author.
E-mail addresses: rrivero@exa.unrc.edu.ar (R.E. Rivero), mmiras@exa.unrc.edu.ar (M.C. Miras), crivarola@exa.unrc.edu.ar (C.R. Rivarola), cbarbero@exa.unrc.edu.ar (C.A. Barbero).

http://dx.doi.org/10.1016/j.reactfunctpolym.2015.10.011
1381-5148/

In this study, we have synthesized poly(N-isopropylacrylamide) PNIPAM-based hydrogels with characterized physicochemical and mechanical properties, thermosensitive capabilities, interconnected macro-superpores, and good cytocompatibility. The obtained results indicate that different functional groups that are present on hydrogels provoke a significant effect on the properties of the polymeric material. In addition, the cytocompatibility of hydrogels makes them appealing scaffold materials for biomolecule production or cell growth, engineering tissue replacements, and a variety of potential applications.

2. Materials and methods

2.1. Materials

Thermosensitive hydrogels were synthesized by free radical polymerization of N-isopropylacrylamide (NIPAM) (Scientific Polymer Products) and copolymerization with different proportions of 2-acrylamido-2-methylpropanesulfonic acid (AMPS) (Scientific Polymer Products) or N-acryloyl-tris-(hydroxymethyl)amino methane (HMA) (Sigma-Aldrich). The chemical structures of the monomers are shown in Scheme 1. N,N-methylenebisacrylamide (BIS) (Sigma-Aldrich) was used as cross-linking agent. Ammonium persulfate (APS) (Sigma-Aldrich) and N,N,N′,N′-tetramethylenediamine (TEMED) (Sigma-Aldrich) were used as polymerization initiators.

2.2. Synthesis of hydrogels at room temperature

The cross-linking agent, BIS (2% moles based on NIPAM) was dissolved in an aqueous solution of NIPAM monomer (0.5 M). Then, polymerization initiators (APS 0.001 g/mL and TEMED 10 μL/mL) were added, and O_2 was purged by bubbling with N_2 gas. The dissolved oxygen (highly reactive) inhibits polymerization for several minutes, and hence a previous purging is necessary. The resulting polymer was PNIPAM network. For copolymeric hydrogel synthesis, a percentage of moles (x) of AMPS or HMA based on moles of NIPAM was added, resulting in cross-linked copolymers PNIPAM-co-x% AMPS and PNIPAM-co-x% HMA, respectively. The polymerization was conducted in a sealed glass tube at room temperature (RT) (20 °C) for 3 h.

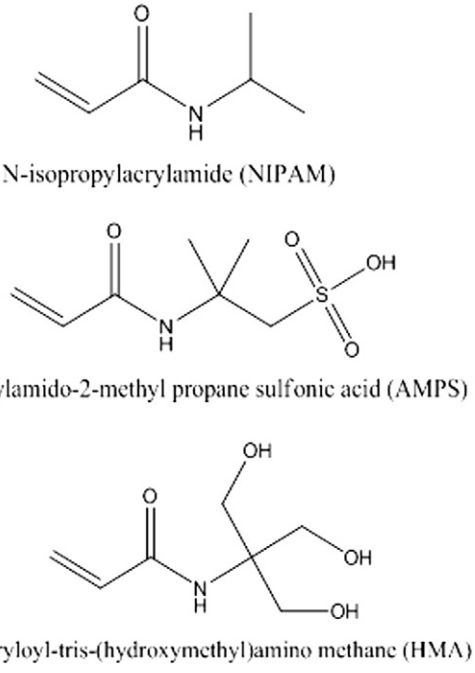

Scheme 1. Chemical structure of the monomers.

After the completion of the polymerization reaction, the hydrogels were immersed in distilled water at RT for 48 h, and the water was replaced several times to remove unreacted chemicals.

2.3. Synthesis of hydrogels by cryogelation

Hydrogels were produced by free radical polymerization at −18 °C using the pre-polymeric solutions described in Section 2.2. In this case, the solution was not purged to inhibit the polymerization reaction before freezing. The initiators were added at 0 °C, and the solution was transferred to a plastic 1-mL syringe and sealed immediately. The loaded syringe was placed in a tubular piece of expanded polystyrene, where it fits tightly, leaving the ends of the syringe free to allow cooling from the syringe barrel. The polystyrene-covered syringe was then placed in a freezer set at −18 °C. The solution was kept undisturbed for 24 h for the reaction to take place. Then, the content of the syringe was thawed at RT, and the wet hydrogel was thoroughly washed with running deionized water to remove unreacted chemicals.

2.4. Physicochemical and mechanical characterization

2.4.1. Study of swelling kinetics

Samples of previously washed hydrogel were dried at reduced pressure and approximately 30 °C, and weighed. Then, they were placed in a distilled water bath at RT. The samples were removed from the water bath at regular intervals, superficially dried using tissue paper, weighed on an analytical scale, and placed again in the water bath. The measurements were repeated until a constant weight was obtained for each sample. The swelling percentage (%Sw) as a function of time was calculated by the following equation:

$$\%Sw(t) = 100 \times [(W(t) - W(to))/W(to)], \quad (1)$$

Where W(t) represents the weight of hydrogel in swollen state at time t and Wo represents the weight of dry hydrogel.

The initial slope, estimated from the %Sw versus time curve, is defined as the initial rate (Ri) for each hydrogel.

2.4.2. Differential scanning calorimetry

Differential scanning calorimetry (DSC) measurements were used to determine the phase transition temperature and analyze the states of water present in the hydrogels. Measurements were conducted using a DSC 2010, purchased from TA Instruments, under N_2 flow. Sealed aluminum capsules were quickly cooled in the calorimeter chamber at −25 °C by filling the outer reservoir with a frozen solution of $CaCl_2$ in water (80% w/w). After several minutes, the system reached equilibrium state. The sample holder assembly was then heated to 60 °C (above the phase transition temperature) at a rate of 10 °C/min. The temperature was maintained below 100 °C to avoid sample water evaporation. The same experimental conditions were used to analyze the states of water.

2.4.3. Analysis of hydrogel morphology by scanning electron microscopy

Scanning electron microscopy (SEM) images were taken at both low vacuum in a LEO 1450VP variable field emission SEM. The measurements were taken in lyophilized hydrogel samples covered with a thin layer of gold by sputtering (2 min at 15 mA).

2.4.4. Determination of elastic modulus (E) by uniaxial compression

Elastic modulus of an object is the slope of stress–strain curve in the elastic deformation region [28]. Stress is the restoring force (F) resulting from the deformation applied divided by the original cross-sectional area (A) to which the force is applied. Strain is the ratio of the change in the length of the object (ΔL) to the length from the original state (Lo) of the object. When ΔL is small, Hooke's law is valid, according to

which stress ε is proportional to strain σ. The constant of proportionality is known as the Young's modulus (E).

Uniaxial compression measurements were taken on individual cylindrical hydrogels in swollen state at 25 ± 0.5 °C. A device, similar to the one described earlier [24,8], was built to measure the modulus under compression. Briefly, a cylindrical hydrogel piece of approximately 0.5 cm in diameter and 1–1.5 cm in height was placed on an analytic digital scale (OHAUS Pioneer, readability and reproducibility of 0.1 mg). A load was transmitted vertically on the hydrogel through a micrometric actuator with a glass end plate. When the glass plate was in contact with the cross-sectional area of the hydrogel cylinder, the scale was tared to zero. Then, a force ($F = m \times g$) was applied on the hydrogel, where m is the mass read on the scale and g is the acceleration due to gravity. The stress ε was calculated as F/A. The resulting deformation was measured using a digital comparator (Schwyz Electronic indicators), which is sensitive to displacements of 10^{-3} mm. The comparator lengths were measured before (L) and after (L1) the application of force, and ΔL was calculated as their difference (L1 − L). The initial length of the hydrogel cylinder (L_0) was measured earlier using an absolute micrometer, and the strain was calculated as $\sigma = \Delta L/L_0$. The force and the resulting deformation were recorded after 30 s of relaxation. During the measurements, the load was increased in successive steps until the gel was deformed up to about 20% compression. By plotting ε against σ, it is possible to calculate the modulus (E) from the slope. The experiments were performed thrice, and the results were averaged.

2.4.5. Effect of oriented pores on elastic modulus of hydrogels

The elastic modulus of hydrogels with oriented ellipsoidal macropores was measured by applying uniaxial compression in two directions: (i) parallel (longitudinal) to the major pore's axis (axial compression) and (ii) perpendicular to the major pore's axis (transverse compression). Therefore, in order to obtain the elastic modulus during hydrogel axial compression, a force parallel to the major axis of the hydrogel cylinder was applied (Scheme 2, left), whereas, to determine the elastic modulus during hydrogel transverse compression, a hydrogel cylindrical piece perpendicular to the major axis of the original hydrogel cylinder was obtained using a metallic punch of 0.5 cm in diameter, such that a cylindrical subsample with similar size (0.5 × 1 cm) was available for compression (Scheme 2, right). E values obtained on directions parallel and perpendicular to ellipsoidal pore's major axis of hydrogel were compared.

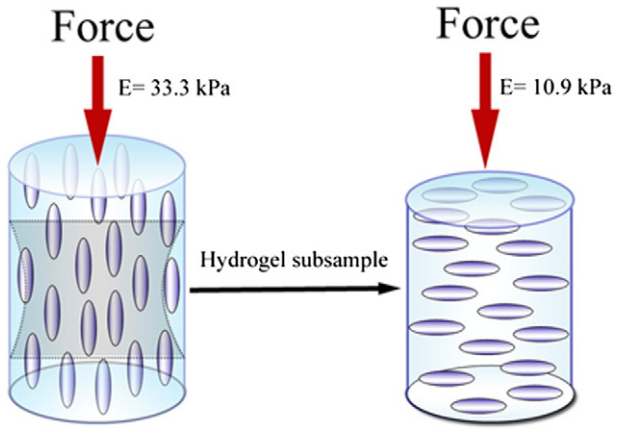

Scheme 2. Schematic of the generation of a cylindrical subsample perpendicular to the major axis of the cylindrical hydrogel (PNIPAM). Subsequently, uniaxial compression force was applied to each hydrogel cylinder, and E is calculated.

2.5. Biological experiments

2.5.1. Cell culture

Hydrogels were hydrated with complete cell culture medium (DMEM, 10% of bovine fetal serum (BFS) and antibiotic-antimitotic) overnight and placed at the bottom of cell culture dishes. BFSs, which constitutively express a green fluorescent protein (GFP) (generously provided by Dr. Wilfried Kues, *Friedrich Loeffler Institute*, Germany), were trypsinized and seeded on hydrogels at a density of 10^5 cells/well in a 24-well plate. The cells were incubated at 37 °C in a humidified atmosphere of 5% CO_2 in air. After 24 h of culture, the morphology of attached cells on each hydrogel was observed in an inverted microscope under UV light (Nikon Ti-S 100, Nikon Japan), and pictures were taken using a digital camera (Nikon, Japan).

2.5.2. Cell viability assay

The effect of hydrogels on cell viability was evaluated by the MTT assay, which measures the conversion of 3-(4,5-dimethylthiazol-2-yl)-2,5-diphenyltetrazolium bromide (MTT) to an insoluble formazan. The formazan was then solubilized, and the concentration was determined by optical density at 540 nm. Briefly, BFs were seeded in a 96-well plate at a density of 5000 cells/well in 100 μL of complete DMEM. The cells were allowed to grow on different hydrogels for 24 h in an incubator at 37 °C in a humidified atmosphere of 5% CO_2. Each experimental condition, including a viability control group in which the hydrogel was omitted, was run in octuplicate. After 24 h of culture, the MTT reagent (5 mg/mL) was added to each well and further incubated for 3 h at the same temperature. The reaction mixture was removed from each well and replaced by 100 μL of dimethyl sulfoxide (DMSO). The absorbance (A) at 540 nm was measured using a microplate reader (Bio-Rad®). The data are shown as mean value ± SD (standard deviation).

3. Results and discussion

3.1. Hydrogel morphologic analysis by SEM

The microscopic structure and characteristics of pores present in hydrogels synthesized at RT and subzero temperatures (cryogelation) were analyzed using SEM. According to the size of pores, Kim and Park [29] classified hydrogels as microporous (10–100 nm), mesoporous (100–1000 nm), macroporous (1–100 μm), and superporous (100–1000 μm).

SEM images show that the hydrogels synthesized at RT have microscale pores (Fig. 1a). Calculations based on Flory–Rehner theory, supported by empirical data, indicate that cross-linked gels have nanoscale pores, and therefore they are classified as compact or nanoporous materials [15]. However, cryogelation process or synthesis at freezing temperature has been used extensively for the fabrication of porous hydrogels in tissue engineering [30]. During the process, the solvent (water) freezes by forming ice crystals, which act as physical templates of the macropores and produce a no frozen microphase around them. This can be explained by a reduction of the freezing point caused by the increase of solute concentration (colligative property). Therefore, the reactant concentration in the unfrozen microphase increases because of the loss of water by freezing, favoring polymerization reaction that proceeds even at low temperatures. In addition, oriented ice crystals in the direction of the gradient are obtained by applying uniaxial gradient of temperature [31,32]. This was achieved by isolating the walls of the polymerization tube with closed-cell extruded polystyrene foam (Styrofoam), driving heat losses at the free extremes.

It has been demonstrated that the initial temperature of the cryogelation reaction in water highly affects the hydrogel structure and properties [33]. For a given initial temperature of cryogelation, the distribution of water molecules during freezing is mainly influenced by the ionic and nonionic groups of the hydrogel components. Indeed,

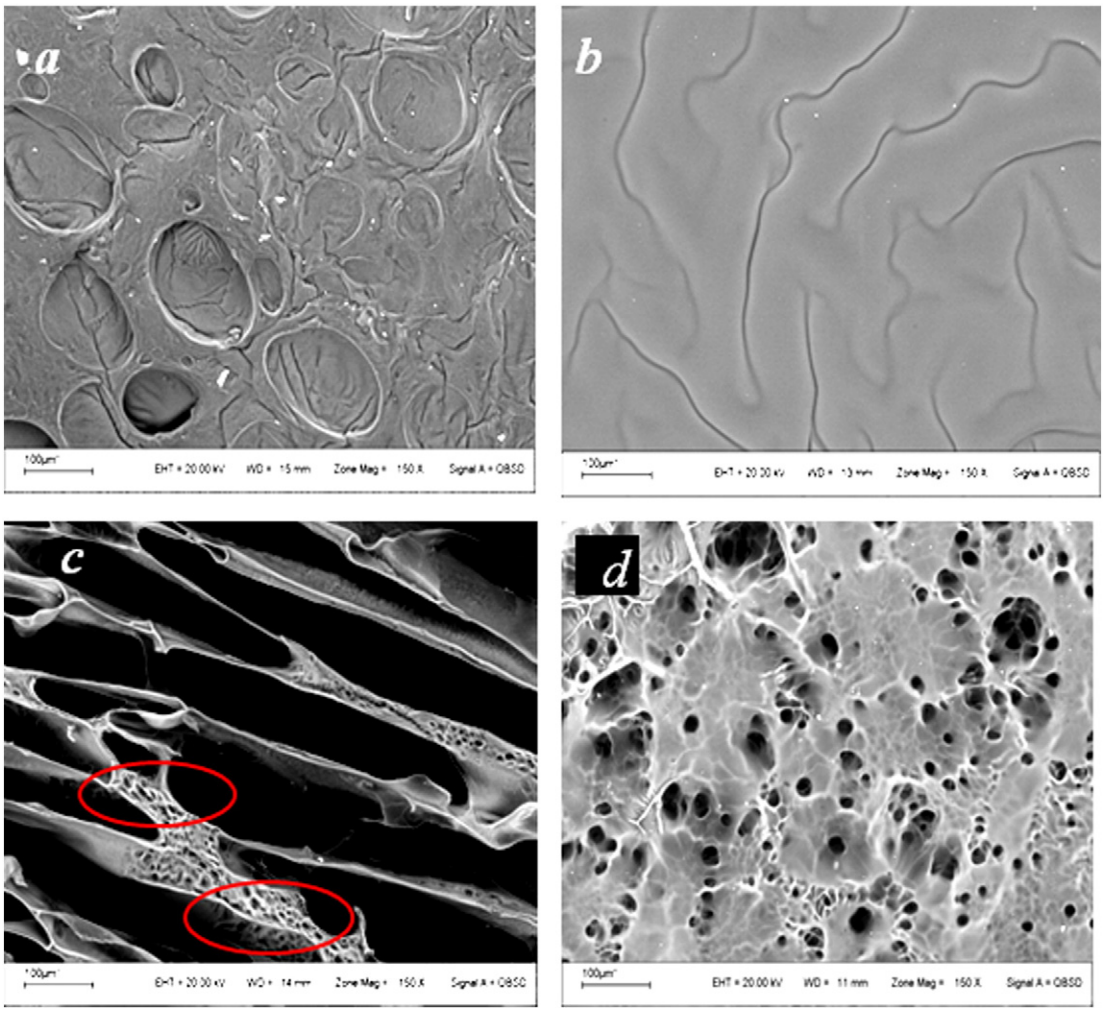

Fig. 1. SEM images of: PNIPAM hydrogel produced at room temperature (a), PNIPAM-co-10% HMA hydrogel produced by cryogelation (b) and PNIPAM-co-2% AMPS hydrogel synthesized by cryogelation in which the hydrogel cylinder is cut longitudinally (c) or transversally (d). Red ovals in (c) represent sub pores that interconnect ellipsoidal macropores. Scale bar: 100 μm.

it is well known that the hydrophilicity of a polymer affects the nucleation of ice [34]. In our study, the initial temperature of the cryogelation reaction was always the same; therefore, the observed arrangement of pores depends on the hydrophilicity of the comonomer used (HMA or AMPS) PNIPAM-co-10% HMA hydrogel shows thick walls with no interconnected spherical pores with diameters of approximately 80–120 μm (Fig. 1b), whereas PNIPAM-co-2% AMPS hydrogel (Fig. 1c) shows interconnected ellipsoidal (rodlike) pores. The detailed morphology of these pores can be observed in SEM images taken in the axial (Fig. 1c) and transversal (Fig. 1d) sections of the hydrogel. These images depict the rodlike morphology with pore minor and major axes of 30–60 and 480–500 μm, respectively. In addition, the rodlike pores are oriented along the major axis of the hydrogel, and the walls have sub pores that interconnect the rodlike macropores (Fig. 1c).

The importance of obtaining accurate hydrogel three-dimensional (3D) structure and pore size for successful cell colonization and proliferation has been emphasized by experiments that demonstrate optimum pore sizes of 5–15 and 100–350 μm for fibroblast growth and bone regeneration, respectively. Growth of fibrovascular tissues also requires pore sizes >500 μm for rapid vascularization and survival of transplanted cells [11]. Therefore, the control of scaffold porosity and microarchitecture plays a key role in determining engineered tissue properties and function.

Identical SEM images are observed for PNIPAM-co-2% AMPS and PNIPAM hydrogels obtained by cryogelation. Considering the infeed ratio of monomers and full conversion reaction, it is possible to analyze the morphologic effect of pores caused by the ratio of functional groups present in the hydrogel. Thus, it is possible to consider the elemental analysis, that is, chemical composition of hydrogels, valuing the ratio of functional groups present in them. PNIPAM-co-2% AMPS presents 50 isopropyl groups for each $-SO_3^-$ group, whereas PNIPAM-co-10% HMA presents 3.3 isopropyl groups for each –OH group. This similarity in the morphologies of PNIPAM and PNIPAM-co-2% AMPS is due to the lower or depreciable amount of AMPS. However, a higher amount of –OH groups considerably affects the formation of water crystal, resulting in a different morphology. It is also possible that this functional groups ratio affects the other physicochemical properties of hydrogels significantly.

3.2. Phase transition temperature and swelling capacity

It is well known that PNIPAM is a thermosensitive hydrogel with a phase transition temperature of approximately 32–33° [36]. The copolymerization of NIPAM with hydrophilic comonomers increases the phase transition temperature. Therefore, we synthesize copolymeric hydrogels based on the combination of NIPAM with different mass ratios of ionic (AMPS) or nonionic (HMA) comonomers. Hydrogel phase transition temperatures (T_{PT}) obtained by DSC are shown in Fig. 2. In agreement with the previous studies [35], a clear relationship between the presence of hydrophilic groups in the polymer chain and the phase

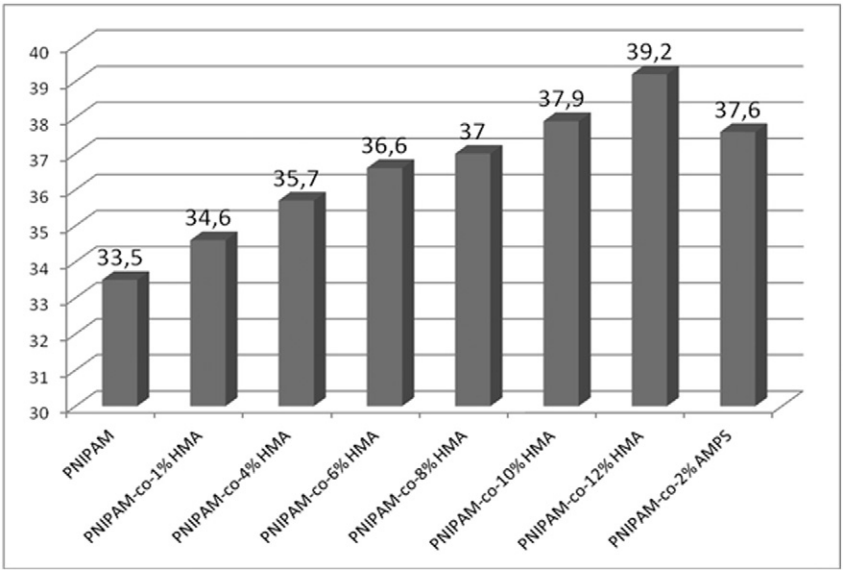

Fig. 2. Phase transition temperatures of the different PNIPAM-based copolymer hydrogels.

transition temperature is observed. In order to achieve the purpose of developing materials that can be applied in the fields of mammalian cell biology and biomedicine, hydrogels with a phase transition temperature almost equal to human body temperature are produced. The introduction of 2% AMPS in PNIPAM chains is sufficient to obtain a hydrogel with T_{PT} around normal human body temperature and almost independent of pH changes [36]; however, the addition of 10% of HMA monomer is required to increase T_{PT} to a similar value. The thermosensitivity of hydrogels generated from copolymerization or PNIPAM alone has been exploited to develop smart drug delivery systems, in which drug release could be induced by thermal heating [4,36] or absorption of electromagnetic radiation (microwave or near-infrared (NIR) light) [24,37] to avoid thermal decomposition of the drug under study.

Once the percentage of each hydrophilic comonomer in the reaction mixture required to generate a hydrogel with a phase transition temperature almost equal to human core body temperature was identified, we aimed to further characterize these hydrogels. Swelling kinetics of hydrogels with T_{PT} around normal human body temperature, synthesized at RT compared with PNIPAM, are shown in Supplementary information (Fig. 1 (SI)). The higher swelling capacity observed in PNIPAM-co-2% AMPS can be explained by the presence of ionic moieties ($-SO_3^- Na^+$), which generate an overall charge density along the chains and high concentration of mobile ions in the hydrogel during dissociation. When sulfonic groups are present, two forces that lead to hydrogel swelling are as follows: (i) the osmotic pressure resulting from differences in ion concentration between the swollen gel and the external solution and (ii) the electrostatic repulsion (i.e., coulombic force) between charged chain segments. In PNIPAM-co-10% HMA, the intermolecular bindings between the hydroxyl groups eventually reduce the hydrogen bonding with water, resulting in a decrease of hydrogel swelling capacity, similar to PNIPAM [38]. It is noteworthy that T_{PT} is not affected by synthetic methods of pore formation (Supplementary information, Table 1(SI)).

Table 1 summarizes the results of swelling initial rate (R_i) and equilibrium swelling percentage ($\%Sw_{eq}$) for PNIPAM, PNIPAM-co-10% HMA, and PNIPAM-co-2% AMPS. The initial swelling rate (R_i) could be related to percentage of porosity (%Ps) of nano- or macroporous materials or the superficial area of material in contact with water. For that reason, the %Ps values of hydrogels were measured by gravimetric method using cyclohexane as solvent, so as to only fill the pores without solvating the polymer chains. Hydrogels obtained by cryogelation showed a higher %Ps than those obtained at RT; however, it seems that the functional groups did not affect this property (Supplementary information, Table 2(SI)). Thus, the increase of the initial swelling rate (R_i) (Table 1) could be due to the presence of hydrophilic functional groups ($-OH$, $-SO_3^-$) in the polymer, as they create a driving force for hydrogel swelling.

However, $\%Sw_{eq}$ is higher for nanoporous hydrogels obtained at RT, probably because the pliability of material allows more intake of water. Rigid pore walls in macro-superporous hydrogels may reduce the hydrogel water loading capacity.

3.3. Analysis of water states

Having a prior knowledge on the physical states of water in the hydrogel will provide useful information about the nature of the physical interactions between the polymer chain and the swelling medium [39]. In general, the water structure in the polymer hydrogel can be categorized as “free water”, “nonfreezing bound water”, and “freezing bound water.” [40].

As the name indicates, free water does not establish hydrogen bonding with polymer molecules and behaves similarly to pure water regarding transition temperature, enthalpy, and DSC curves. By contrast, nonfreezing bound water is the fraction of water that forms hydrogen bonds with the polymer chain. Finally, freezing bound water interacts weakly with polymer molecules. The total content of freezing water ($W_{freezing}$) was calculated using DSC, from the area under the

Table 1
Initial swelling rate (R_i) and equilibrium swelling percentage ($\%Sw_{eq}$) of PNIPAM and copolymer hydrogels synthesized by different methods.

Hydrogel (synthetic method)	Ri (%Sw/min)	$\%Sw_{eq}$ (± 200) (± 100)
PNIPAM (RT)	18.4	2600
PNIPAM (Cry)	48.9	1900
PNIPAM-co-10% HMA (RT)	22.7	2300
PNIPAM-co-10% HMA (Cry)	18.3	2100
PNIPAM-co-2% AMPS (RT)	52.9	5300
PNIPAM-co-2% AMPS (Cry)	83.6	4800

RT: hydrogel synthesized at room temperature.
Cry: hydrogel synthesized by cryogelation.

endothermic curve for water-swollen hydrogels (Q_{endo}) to endothermic heat of fusion for pure water ($Q_{pw} = 333.3$ J/g).

$$W_{freezing}\ (\%) = W_f + W_{fb} = (Q_{endo}/Q_{pw}) \times 100, \quad (2)$$

where W_f and W_{fb} are the fraction of free water and freezing bound water, respectively.

The content of nonfreezing bound water (W_{nfb}) can be indirectly determined as the difference between equilibrium water content (EWC) and $W_{freezing}$:

$$EWC = [(w_s - w_d)/w_s] \times 100 \quad (3)$$

$$W_{nfb} = EWC - W_{freezing} \quad (4)$$

Where w_s is the weight of the hydrogel sample in the swollen equilibrium state and w_d is the weight of the dried gel.

The results obtained from DSC melting endothermic peak on heating run for each hydrogel are summarized in Table 2, and the calculated mean values are presented. Their statistical errors were all within 5%.

For hydrogels obtained at RT (nonporous), $W_{freezing}$ is higher for PNIPAM-co-10% HMA than for PNIPAM and PNIPAM-co-2% AMPS, where isopropyl groups are present in a higher proportion. This is likely due to the larger amount of hydrophilic (−OH) than hydrophobic (isopropyl) groups in PNIPAM-co-10% HMA. This result indicates that the –OH groups of PNIPAM-co-10% HMA interact each other mainly through hydrogen binding, rather than with free water. By contrast, macro-superporous hydrogels obtained by cryogelation increase the content of nonfreezing bound water (W_{nfb}) or the amount of water interacting with the polymer chains by increasing the number of hydrogen bonds. Presumably, this marked difference in W_{nfb} content may be the result of the larger superficial area in macro-superporous hydrogels in contact with the aqueous medium.

The DSC measurements of PNIPAM-co-2% AMPS hydrogels in Fig. 3 show that when the hydrogel is obtained at RT and by cryogelation, melting of water occurs at temperatures >0 and <0 °C, respectively. Because of a change in colligative properties of water, it is possible for sulfonic groups to be more exposed to the surface of pores and the sulfonate ions and/or the counterions to induce a reduction in the freezing point. In addition, two peaks are observed below 0 °C in macroporous PNIPAM-co-2% AMPS hydrogel, indicating the presence of the aforementioned three different kinds of water, which can in turn be explained by the simultaneous presence of nano and macropores in the material (Fig. 1c). The three different states of water were only detected in hydrogels made by cryogelation (Supplementary information, Fig. 2 (SI)) regardless of the comonomer used (AMPS or HMA), suggesting that the presence of pores but neither their shape nor size affects the state of water in the gel. Similarly, Baba et al. [41] reported the presence of the three states of water in *polyethylene glycol* (PEG) and polyvinyl alcohol (PVA) hydrogels, in which a heterogeneous gel phase consisting of hydrated polymer domains and macropores with relatively hydrophobic surface is present. In these hydrogels, the freezable bound water was considered as water isolated in small pores of the hydrophobic domains.

Table 2
States of water in hydrogels calculated from DSC measurements.

Hydrogel (Synthetic method)	Q_{endo} (J/g)	EWC (%)	$W_{freezing}$ (%)	W_{nfb} (%)
PNIPAM (RT)	115.2	97.5	34.5	62.9
PNIPAM-co-10% HMA (RT)	200.8	95.8	60.3	35.5
PNIPAM-co-2% AMPS (RT)	183.5	97.8	55.1	42.7
PNIPAM (Cry)	61.7	95.4	18.5	76.9
PNIPAM-co-10% HMA (Cry)	168.7	96.1	50.6	45.4
PNIPAM-co-2% AMPS (Cry)	7.9	97.1	2.4	94.7

RT: hydrogel synthesized at room temperature.
Cry: hydrogel synthesized by cryogelation.

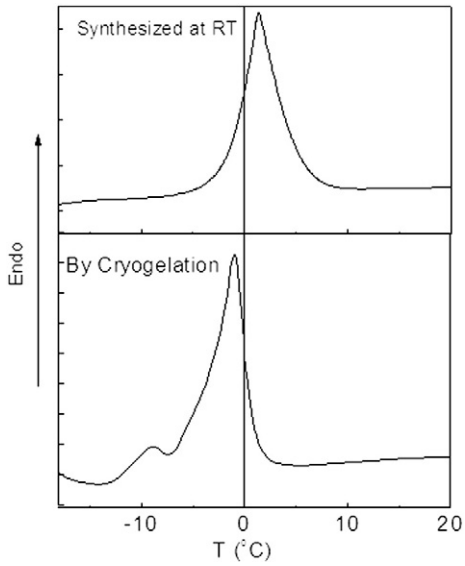

Fig. 3. DSC heating curves of water absorbed in PNIPAM-co-2% AMPS synthesized by different methods.

3.4. Elastic modulus determined by uniaxial compression

Considering the morphological characteristics of hydrogels, it is expected that the mechanical properties would be affected by the shape and size of pores. Elasticity is a property that describes the tendency of a material to deform elastically (i.e., no permanently) when a force is applied on it. A stiff material would have a higher value of elastic modulus (E).

Fig. 4 shows the compressive stress–strain curve determined under uniaxial compression on PNIPAM and PNIPAM-co-2% AMPS, synthesized at RT or by cryogelation at −18 °C. It is evident from the figure that the hydrogels obtained by cryogelation show a steeper slope, suggesting that the walls of pores are more rigid than hydrogels obtained at RT. This shows that zones of high monomer concentration produced during freezing induce the formation of stiffer polymer walls.

The elastic moduli (E) of all the hydrogels studied are presented in Table 3. E values of hydrogels synthesized at RT ranged between 3 and 6.5 kPa, which are lower than those reported for rigid polymeric materials [42]. Of the hydrogels synthesized at RT, PNIPAM-co-2% AMPS has the largest E value. This may be due to ion-dipole interactions in PNIPAM-co-2% AMPS, which would in turn increase the rigidity of the material.

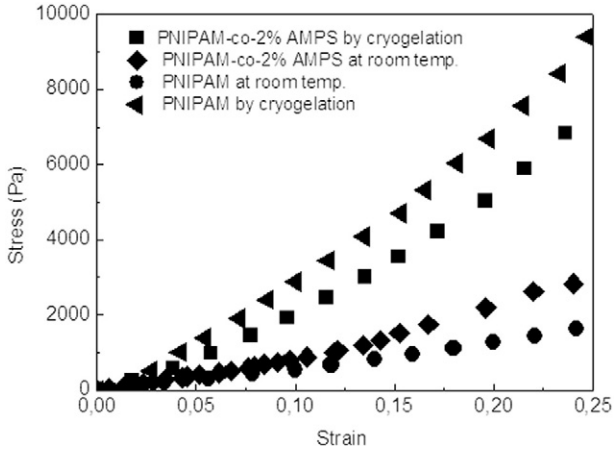

Fig. 4. Compressive stress–strain curve for PNIPAM and PNIPAM-co-2% AMPS hydrogels obtained under uniaxial compression.

Table 3
Elastic modulus (E) determined by uniaxial compression.

Hydrogel (synthetic method)	E[a] measured (kPa)
PNIPAM (RT)	5.9
PNIPAM (Cry)	33.3
PNIPAM-co-10% HMA (RT)	5.9
PNIPAM-co-10% HMA (Cry)	3.1
PNIPAM-co-2% AMPS (RT)	6.6
PNIPAM-co-2% AMPS (Cry)	20.5

RT: hydrogel synthesized at room temperature.
Cry: hydrogel synthesized by cryogelation.
[a] Experimental value (+/− 0.5 kPa).

It is noteworthy that PNIPAM and PNIPAM-co-2% AMPS hydrogels synthesized by cryogelation had elastic modulus significantly larger than that calculated for PNIPAM-co-10% HMA. We hypothesized that the longitudinal pores generated during cryogelation are responsible for the mechanical behavior observed of hydrogels.

3.4.1. Effect of oriented rod-like pores in hydrogels on mechanical response to uniaxial compression

The presence of oriented rodlike macropores in PNIPAM and PNIPAM-co-2% AMPS synthesized by cryogelation, leads to the hypothesis that the hydrogels respond anisotropically to compression.

In order to test this hypothesis, the elastic modulus was estimated when compression force was applied parallel or perpendicular to the ellipsoidal pore's major axes (Scheme 2). The value of modulus (E) of PNIPAM obtained by the application of force on the direction perpendicular to the rod-like pores (transversal compression) was significantly lower (10.9 kPa) than that obtained with axial compression (direction parallel to pore's major axis) (33.3 kPa, Table 3). Similar results were obtained for PNIPAM-co-2% AMPS, that is, transversal modulus (perpendicular to major axis) of 12.1 kPa and longitudinal modulus (parallel to major axis) of 20.5 kPa.

These results demonstrated that the elastic modulus of porous hydrogels depends on shape, size, and orientation of the pores. Bones and cartilage exhibit similar anisotropic mechanical behavior, displaying a higher mechanical resistance axially than transversally [43]. Therefore, these hydrogels could be suitable materials to build 3D scaffolds for hard tissue engineering.

Gibson and Ashby [44] developed an experimentally verified model for anisotropic porous structures [45]. For an anisotropic open-pore foam [46], with struts of thickness t and lengths h and l in the longitudinal and transverse directions, respectively, they calculated the ratios of longitudinal (E_L) to transverse (E_T) modulus as.

$$r_{L/T} = E_L/E_T = 2(DA)^2/\left(1 + (1/DA)^3\right), \quad (5)$$

where DA = h/l.

Considering the E values obtained, the value of $r_{L/T}$ was calculated as 3.05 for PNIPAM on each direction to longitudinal pore axis, whereas the value was 1.69 for PNIPAM-co-2% AMPS. A substantial anisotropic behavior was observed by Hoffmeister et al. [47] in Young's modulus in the plane containing the long axis of the human tibia. They reported the values of $r_{L/T}$ to be approximately 1.7. Therefore, this natural mechanical property of tibial bone could be mimicked by PNIPAM-based hydrogels with rodlike macropores.

3.5. Adhesion and viability of BFs growing on hydrogel surfaces

Microscopic images taken under UV light 24 h after cell seeding showed marked morphologic differences between the cells attached to PNIPAM-co-2% AMPS and those growing on conventional polystyrene culture surface (control) attached to PNIPAM and PNIPAM-co-10% HMA (Fig. 5). Often, cell adhesion is associated with hydrophobic/hydrophilic properties of the surface [48,49]. Studies of contact angles on hydrogels showed that PNIPAM (84.0°) exhibits hydrophobic characteristic, PNIPAM-co-10% HMA (66.4°) is just under-hydrophobic, and PNIPAM-co-2% AMPS (30.5°) is hydrophilic. Images of contact angle are presented in Supplementary information (Fig. 3 (SI)). Therefore, the morphology of attached cells is in agreement with hydrophobicity of the hydrogel surface. However, it seems that the presence of anionic groups ($-SO_3^-$ of AMPS) decreases the matrix-cell interactions, and hence the cells tend to group in small clumps fixed on the gel (Fig. 5b) initially. On the contrary, nonionic hydrophilic groups, such as –OH of HMA or amide of PNIPAM, on the hydrogel surfaces stimulate the matrix-cell interactions as was evidenced by the classic spindle shape of the attached bovine fibroblasts (BFs) (Fig. 5a and c). Starting on day 15 after cell seeding on PNIPAM-co-2% AMPS hydrogel, cell clumps observed during the early days of culture were progressively despairing (Supplementary information, Fig. 4 (SI)). This could be interpreted as a cell adaptation to the hydrogel surface or a physicochemical change of the hydrogel surface that made it a more amenable substrate for cell adherence. However, future studies are required to confirm such effect.

The use of hydrogels as biological scaffolds for tissue engineering and regenerative therapy implies that the material not only provides support for cell attachment and proliferation, but also it is innocuous to the cells. Therefore, we aimed at studying the effect of hydrogels on cell viability using the classic MTT assay. No toxic effect, or putative soluble molecules released to the medium, was observed in the hydrogels under study (Fig. 5e). Surprisingly, a mild proliferative effect was observed in BFs growing on PNIPAM and PNIPAM-co-10% AMPS hydrogels. The causes and biological significance of the proliferative effect detected in BFs attached to these hydrogels warrant further studies.

4. Conclusions

The phase transition temperature and physicochemical characteristics of PNIPAM hydrogel can be altered by copolymerization with hydrophilic monomers (2% AMPS or 10% HMA). Depending on the hydrophilicity of comonomer functional groups, it is possible to obtain hydrogels with oriented macro-superpores or isolated spherical macropores by cryogelation. In hydrogels with oriented ellipsoid-shaped pores, axial mechanical resistance was observed to be higher than the transversal counterpart, similarly to the mechanical behavior of hard tissues such as cartilage and bone [47,48].

PNIPAM-based hydrogels can support fibroblast cell attachment and proliferation for extended periods of time (up to 20 days) without any significant cytotoxic effect. These results warrant more studies aiming at further characterizing other biological aspects of these hydrogels, such as cell migration into the gel matrix, in vivo immune tolerance, and biodegradability. Similarly, the thermosensitivity almost equal to human body temperature allows the use of these materials as both tissue scaffolds and pharmaceutical drug release device [4] for antibiotic, anti-inflammatory, antiseptic, and other biologically active substances in the site of implantation.

It is also possible to control the mechanical properties of hydrogel by selecting comonomers and temperatures during synthesis (RT or cryogelation), without losing hydrogel sensitivity to the set temperature. The fact that the synthesized material has different elastic moduli during axial and transversal compressions paves the way for its application in biomedicine and other areas, such as industrial technology, as pressure or flow variation sensors.

The cytocompatibility and particular mechanical response of hydrogels with oriented macro-super pores produced in this study make them good materials for developing engineered cellular 2D- or 3D-cell scaffolds, as similar materials based on polyacrylamides [50–55].

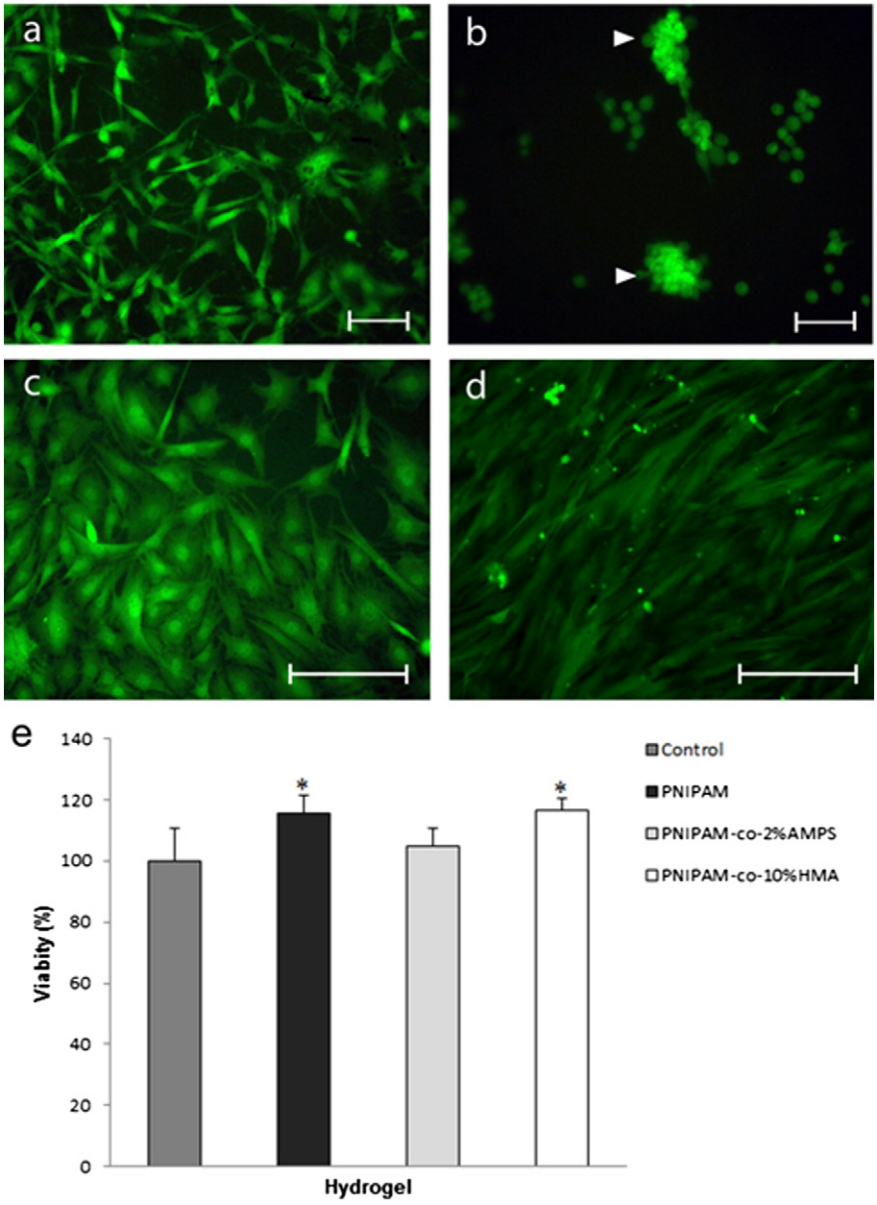

Fig. 5. Microphotographs of bovine fibroblast (BF) attached to PNIPAM (a), PNIPAM-co-2% AMPS (b), and PNIPAM-co-10% HMA (c) hydrogels. Pictures were taken under UV light 24 h after cell seeding. Cells exhibit a typical fibroblastic morphology when attached to PNIPAM (a) and PNIPAM-co-10% HMA (c), but they form cell clumps when adhered to the PNIPAM-co-2% AMPS hydrogel (b, arrowheads). For comparison, BFs growing on conventional culture surface (polystyrene) cells are shown in (d). Scale bar: 50 μm. (e) MTT viability assay of FBs on different hydrogels after 24 h of culture. * indicates statistical differences from the control ($p < 0.05$, ANOVA and Tukey). Data represents media ± SD.

Acknowledgments

This study was funded by FONCYT PICT 2011-1701, CONICET PIP 11220120100529CO, SECYT-UNRC PPI 102a, and John Simon Guggenheim Memorial Foundation. F. Mucklich and F. Soldera (U. Saarlandes) are thanked for their assistance in FE-SEM measurements. The authors also wish to thank the European Union (IRSES project "SUMA2-Network", Pr. No: 318903) for the financial support in scientist's mobility.

Appendix A. Supplementary data

Supplementary data to this article can be found online at http://dx.doi.org/10.1016/j.reactfunctpolym.2015.10.011.

References

[1] B. Mattiasson, A. Kumar, I. Galaev, Macroporous Polymers: Production Properties and Biotechnological/Biomedical Applications, CRC Press/Taylor & Francis, 2009.
[2] J.M. Varghese, Y.A. Ismail, C.K. Lee, K.M. Shin, M.K. Shin, S.I. Kim, I. So, S.J. Kim, Sensors Actuators B Chem. 135 (2008) 336–341.
[3] C. Wachiralarpphaithoon, Y. Iwasaki, K. Akiyoshi, Biomaterials 28 (2007) 984–993.
[4] M.A. Molina, C.R. Rivarola, C.A. Barbero, Polymer 53 (2012) 445–453.
[5] X. Ma, Y. Li, W. Wang, Q. Ji, Y. Xia, Eur. Polym. J. 49 (2013) 389–396.
[6] N. Annabi, J.W. Nichol, X. Zhong, C. Ji, S. Koshy, A. Khademhosseini, F. Dehghani, Tissue Eng. Part B Rev. 16 (2010) 371–383.
[7] M.M. Ozmen, M.V. Dinu, E.S. Dragan, O. Okay, J. Macromol. Sci., Part A: Pure Appl. Chem. 44 (2007) 1195–1202.
[8] F. Topuz, O. Okay, React. Funct. Polym. 69 (2009) 273–280.
[9] A. Kumar, A. Srivastava, Nat. Protoc. 5 (2010) 1737–1747.
[10] J. Hao, R. Weiss, Polymer 54 (2013) 2174–2182.
[11] V.M. Gun'ko, L.I. Mikhalovska, I.N. Savina, R.V. Shevchenko, S.L. James, P.E. Tomlins, S.V. Mikhalovsky, Soft Matter 6 (2010) 5351–5358.

[12] G. Huang, L. Wang, S. Wang, Y. Han, J. Wu, Q. Zhang, F. Xu, T.J. Lu, Biofabrication 4 (2012) 042001.
[13] Y. Hwang, C. Zhang, S. Varghese, J. Mater. Chem. 20 (2010) 345–351.
[14] L. Hockaday, K. Kang, N. Colangelo, P. Cheung, B. Duan, E. Malone, J. Wu, L. Girardi, L. Bonassar, H. Lipson, Biofabrication 4 (2012) 035005.
[15] I. Galaev, B. Mattiasson, Smart Polymers: Applications in Biotechnology and Biomedicine, CRC Press, 2007.
[16] Y. Qiu, K. Park, Adv. Drug Deliv. Rev. 64 (2012) 49–60.
[17] W. Song, X. Yu, D.C. Markel, T. Shi, W. Ren, Biofabrication 5 (2013) 035006.
[18] L. Dong, A.K. Agarwal, D.J. Beebe, H. Jiang, Nature 442 (2006) 551–554.
[19] S. Vijayasekaran, J. Fitton, C. Hicks, T. Chirila, G. Crawford, I. Constable, Biomaterials 19 (1998) 2255–2267.
[20] M. Kobayashi, J. Toguchida, M. Oka, Biomaterials 24 (2003) 639–647.
[21] T.R. Hoare, D.S. Kohane, Polymer 49 (2008) 1993–2007.
[22] Y. Zhang, S. Kato, T. Anazawa, Smart Mater. Struct. 16 (2007) 2175.
[23] Y. Zhang, S. Kato, T. Anazawa, Sensors Actuators B Chem. 129 (2008) 481–486.
[24] R.E. Rivero, M.A. Molina, C.R. Rivarola, C.A. Barbero, Sensors Actuators B Chem. 190 (2014) 270–278.
[25] Z. Yang, Z. Cao, H. Sun, Y. Li, Adv. Mater. 20 (2008) 2201–2205.
[26] C. Sayil, O. Okay, Polym. Bull. 48 (2002) 499–506.
[27] M.A. Cole, N.H. Voelcker, H. Thissen, H.J. Griesser, Biomaterials 30 (2009) 1827–1850.
[28] D. Askeland, P. Fulay, The Science & Engineering of Materials, Cengage Learning, 2005.
[29] D. Kim, K. Park, Polymer 45 (2004) 189–196.
[30] B. Mattiasson, A. Kumar, I.Y. Galeaev, Macroporous Polymers: Production Properties and Biotechnological/Biomedical Applications, CRC Press, 2009.
[31] S. Stokols, M.H. Tuszynski, Biomaterials 25 (2004) 5839–5846.
[32] H. Bai, A. Polini, B. Delattre, A.P. Tomsia, Chem. Mater. 25 (2013) 4551–4556.
[33] M.M. Ozmen, O. Okay, React. Funct. Polym. 68 (2008) 1467–1475.
[34] M. Oguni, C. Angell, J. Phys. Chem. 87 (1983) 1848–1851.
[35] C. de las Heras Alarcón, S. Pennadam, C. Alexander, Chem. Soc. Rev. 34 (2005) 276–285.
[36] M. Molina, C. Rivarola, C. Barbero, Eur. Polym. J. 47 (2011) 1977–1984.
[37] M. Molina, C. Rivarola, M. Miras, D. Lescano, C. Barbero, Nanotechnology 22 (2011) 245504.
[38] N. Saito, T. Sugawara, T. Matsuda, Macromolecules 29 (1996) 313–319.
[39] S.J. Kim, S.J. Park, S.I. Kim, React. Funct. Polym. 55 (2003) 61–67.
[40] T. Goda, J. Watanabe, M. Takai, K. Ishihara, Polymer 47 (2006) 1390–1396.
[41] T. Baba, R. Sakamoto, M. Shibukawa, K. Oguma, J. Chromatogr. A 1040 (2004) 45–51.
[42] R.J. Young, P.A. Lovell, Introduction to Polymers, Third ed. Taylor & Francis, 2011.
[43] J. Williams, J. Lewis, J. Biomech. Eng. 104 (1982) 50–56.
[44] L.J. Gibson, M.F. Ashby, Cellular Solids: Structure and Properties, Cambridge university press, 1997.
[45] J. Jurvelin, M. Buschmann, E. Hunziker, Proc. Inst. Mech. Eng. H J. Eng. Med. 217 (2003) 215–219.
[46] A. Huber, L. Gibson, J. Mater. Sci. 23 (1988) 3031–3040.
[47] B.K. Hoffmeister, S.R. Smith, S.M. Handley, J.Y. Rho, Med. Biol. Eng. Comput. 38 (3) (2000) 333–338.
[48] T. Ishizaki, N. Saito, O. Takai, Langmuir 26 (11) (2010) 8147–8154.
[49] T.A. Horbett, J.J. Waldburger, B.D. Ratner, A.S. Hoffman, J. Biomed. Mater. Res. 22 (5) (1988) 383–404.
[50] M. Constantin, S. Bucatariu, P. Ascenzi, B.C. Simionescu, G. Fundueanu, React. Funct. Polym. 84 (2014) 1–9.
[51] T. Loth, R. Hennig, C. Kascholke, R. Hötzel, M.C. Hacker, React. Funct. Polym. 73 (11) (2013) 1480–1492.
[52] M. Jaiswal, S. Lale, N.G. Ramesh, V. Koul, React. Funct. Polym. 73 (11) (2013) 1493–1499.
[53] G.L. Puleo, F. Zulli, M. Piovanelli, M. Giordano, B. Mazzolai, L. Beccai, L. Andreozzi, React. Funct. Polym. 73 (9) (2013) 1306–1318.
[54] T. Wang, W. Sun, X. Liu, C. Wang, S. Fu, Z. Tong, React. Funct. Polym. 73 (5) (2013) 683–689.
[55] M.V. Dinu, M.M. Perju, E.S. Drăgan, React. Funct. Polym. 71 (8) (2011) 881–890.